EARTH SCIENCES
RESEARCH JOURNAL
Earth Sci. Res. J. Vol. 30, No. 2 (June, 2026): 223 - 229

UNIVERSIDAD NACIONAL DE COLOMBIA

SEISMOLOGY

Seismogenic structure of the 26 March 2025 Yongqing M_L4.6 earthquake and its implication for seismic hazard assessment

Li Deng[1], Yipei Tan[1], Shengxue Lei[1*], Ting Ma[1], Benedict Johnson[2]
1. Tianjin Earthquake Agency, Tianjin, China
2. Department of Earth Sciences, University of Oxford, Oxford, UK

*Corresponding author: dengli@tj.gov.cn

ABSTRACT

Despite being an economically developed sedimentary basin with significant oil and gas production, the North China Plain exhibits anomalously high intraplate seismicity for a densely populated region. On 26 March 2025, a M_L4.6 earthquake struck Yongqing County, following a similar M_L4.8 event in 2018. Both earthquakes occurred near the epicentral region of the devastating 1679 M8 Sanhe-Pinggu earthquake and the seismically active Tianjin Gap, thus drew widespread public attention due to their tectonic implications. This paper conducted a comprehensive investigation of the 2025 Yongqing earthquake's seismogenic structure through the following points. (1) Focal mechanisms inversion for the mainshock and three M_L≥2.5 aftershocks, (2) the earthquake relocation by waveform cross-correlation, and (3)the rupture direction estimation by centroid relative relocation and the spectral ratio technique. The results reveal that the 2025 M_L4.6 earthquake ruptured a NE-striking, steeply dipping right-lateral strike-slip fault, with predominant SW-to-NE rupture propagation. This kinematic behavior shows striking similarity to the 2018 M_L4.8 event, suggesting potential structural linkage. While both seismogenic faults remain unmapped in regional geological surveys, they potentially link with the Xiadian fault zone at mid-crustal levels. Nevertheless, our analysis reveals no conclusive evidence of structural continuity between these faults and the 1679 Sanhe-Pinggu earthquake rupture zone. The nearby Late Pleistocene-active Hexiwu Fault, which has historically produced only one M~5.5 earthquake recorded but exhibits persistent moderate seismicity, may be capable of generating larger ruptures in the future, highlighting the necessity for intensified seismic monitoring within this area.

Keywords: Yongqing earthquake; Seismogenic structure; Focal mechanism; Earthquake relocation; Rupture directivity; North China Plain; Seismic hazard assessment; Xiadian fault zone.

Estructura sismogénica del terremoto M_L4.6 de Yongqing del 26 de marzo de 2025 y su implicación para la evaluación del peligro sísmico

RESUMEN

A pesar de ser una cuenca sedimentaria económicamente desarrollada con una importante producción de petróleo y gas, la Llanura del Norte de China presenta una sismicidad intraplaca anómalamente alta para una región densamente poblada. El 26 de marzo de 2025, un terremoto de magnitud M_L4.6 sacudió el condado de Yongqing, tras un evento similar de M_L4.8 en 2018. Ambos terremotos ocurrieron cerca de la región epicentral del devastador terremoto de M8 Sanhe-Pinggu de 1679 y de la activa brecha sísmica de Tianjin, lo que atrajo una gran atención pública por sus implicaciones tectónicas. Este artículo realizó una investigación exhaustiva de la estructura sismogénica del terremoto de Yongqing de 2025 a través de los siguientes puntos: (1) inversión de los mecanismos focales para el sismo principal y tres réplicas de M_L≥2.5, (2) relocalización del terremoto mediante correlación cruzada de formas de onda y (3) estimación de la dirección de ruptura mediante relocalización relativa del centroid y la técnica de relación espectral. Los resultados revelan que el terremoto ML4.6 de 2025 rompió una falla de deslizamiento lateral derecho con rumbo NE y buzamiento pronunciado, con una propagación de ruptura predominante de SW a NE. Este comportamiento cinemático muestra una notable similitud con el evento M_L4.8 de 2018, lo que sugiere una posible conexión estructural. Aunque ambas fallas sismogénicas no están cartografiadas en los estudios geológicos regionales, podrían estar vinculadas con la zona de falla Xiadian a niveles medios de la corteza. Sin embargo, nuestro análisis no revela evidencia concluyente de continuidad estructural entre estas fallas y la zona de ruptura del terremoto Sanhe-Pinggu de 1679. La cercana Falla Hexiwu, activa durante el Pleistoceno tardío, que históricamente solo ha producido un terremoto registrado de M~5.5 pero muestra una sismicidad moderada persistente, podría ser capaz de generar rupturas mayores en el futuro, lo que resalta la necesidad de intensificar la monitorización sísmica en esta área.

Palabras clave: terremoto de Yongqing; estructura sismogénica; mecanismo focal; relocalización de terremotos; directividad de ruptura; Llanura del Norte de China; evaluación del peligro sísmico; zona de falla Xiadian.

Record
Manuscript received: 14/04/2026
Accepted for publication:

How to cite this item:
Deng, L., Tan, Y., Lei, S., Ma, T., & Johnson, B. (2026). Seismogenic structure of the 26 March 2025 Yongqing ML4.6 earthquake and its implication for seismic hazard assessment. *Earth Sciences Research Journal*, 30(2), 223-229. https://doi.org/10.15446/esrj.v30n2.127009

1. Introduction

Compared to the Tibetan Plateau or Sichuan-Yunnan provinces in Western China, the North China Plain hosts relatively few earthquakes. However, it is marked by unusually high intraplate seismicity (e.g., Li et al., 2007; Liu et al., 2011). Several strong and even devastating earthquakes were recorded in this area. Notable events include the 1679 Sanhe-Pinggu M~8, 1966 Xingtai M7.2, and 1976 Tangshan M7.8 events (Fig. 1), all of which caused severe casualties and tremendous economic losses. The 1976 Tangshan earthquake remains one of the deadliest earthquakes claiming over 240,000 lives and leaving a lasting psychological impact on survivors. Although controversial, a potential seismic gap of approximately M~7 (named "Tianjin Gap") was proposed to the southwest of Tianjin in the North China Plain (Yin et al., 2015), based on historical seismicity, active fault investigations, and GPS observations. Given high population density (~36 million in Beijing and Tianjin combined) and the region's substantial economic importance, even moderate earthquakes are cause for significant public concern.

According to the China Earthquake Networks Center (CENC), a M_L4.6 earthquake struck Yongqing County, Hebei Province, in the North China Plain, on 26 March 2025 (Fig. 1). The epicenter of the earthquake is ~40km southeast of Beijing and ~50km west of Tianjin, but many people in the two cities felt the quake. Before this event, a M_L4.8 earthquake also occurred in the Yongqing county, ~ 8km to the SE of the 2025 event (Fig. 1b), on 12 February 2018. The epicenters of the two events lie 20-30 km SW of the causative fault of the 1679 Sanhe-Pinggu M~8 earthquake (Fig.1b). Historical records suggest that an estimated M5.5 earthquake occurred in Langfang city in A.D.1621 (Li and Li, 2021), 11-15km NE of these two moderate earthquakes (Fig. 1b). Importantly, the two events are very close to the proposed Tianjin Gap (Yin et al., 2015). Therefore, following questions arise as follows: (1) What is the seismogenic structure of the 2025 Yongqing earthquake? (2) What is the tectonic relationship between moderate earthquakes and the 1679 Sanhe-Pinggu event? and (3) What is the future seismic risk in this area?

To address the questions above, this paper first determined the focal mechanism for the mainshock and three M_L≥2.5 aftershocks of the 2025 Yongqing earthquake. Following this, this paper explored the possible seismogenic structure by earthquake relocation using waveform cross-correlation and by rupture directivity analysis using centroid relative relocation and spectral ratio analysis. Combined these results with previous results of the 2018 earthquake and active fault investigation in the region, this paper further examined the tectonic connections among the two moderate earthquakes and the 1679 Sanhe-Pinggu earthquake. Ultimately, this paper assessed the potential seismic risks in this region.

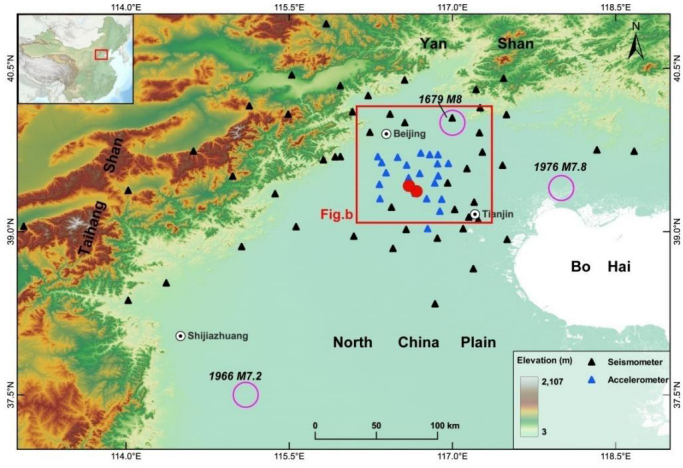

(a)

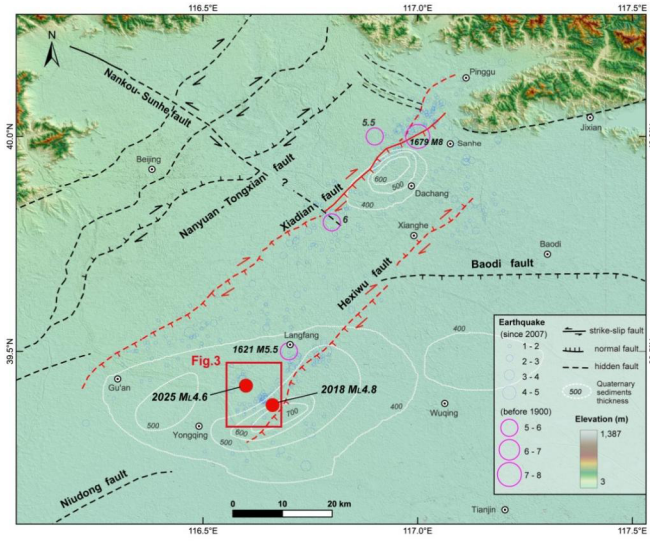

(b)

Figure 1. (a) Locations of the seismometer (black triangle), accelerometer (blue triangle), and large historical earthquake (purple circle). The 2025 and 2018 Yongqing earthquakes are shown in red dots. The historical earthquake catalogue is from Li and Li, 2021. The inset at top left indicates the location of the study region in China. Shan (e.g., Taihang Shan) means Mountain or hill in Chinese. (b) The 2025 Yongqing earthquake and geological setting. Major hidden faults are from Liu et al. (2011), which indicated by black dashed lines, while the Xiadian and Hexiwu faults are highlighted in red. Historical earthquakes (M≥5) are shown in purple circles. Modern instrumentally recorded earthquakes (since 2007) are shown in blue circles. Data of Quaternary sediments thickness are shown in white lines from Liu et al. (2011). The location of Fig.3 is indicated by red box.

2. Geological Setting

The North China Plain has one of the world's most extensive historical earthquake records, with the catalog considered to be complete for M ≥ 6 events since A.D.1300 (Huang et al., 1994). During the early Cenozoic, the North China Plain has undergone extensive east-west extensional tectonics and rifting, resulting in the development of a distinctive basin-range system characterized by NNE-oriented normal faults and corresponding graben and half-graben formations (e.g., Chen et al., 1988). Since the Pliocene, the regional stress field has transitioned to a NE-SW compressional regime, possibly due to the (partial) effect of the India-Eurasia collision (e.g., Feng et al., 2022), resulting right-lateral strike-slipping with (minor) normal component along the pre-existing NNE-trending faults (Zhang et al., 2003). Notably, both major historical earthquakes and modern instrumental seismicity predominantly occurred along NE-trending faults (Chen et al., 1988; Liu et al., 2011). For example, the 1668Tancheng M~8.5, Sanhe-Pinggu, and Tangshan earthquakes occurred along the NE-striking Tan-Lu, Xiadian, and Tangshan faults, respectively.

The Xiadian fault (Fig. 1b) has been suggested to be the seismogenic structure of the 1679 Sanhe-Pinggu M~8 earthquake (Xiang et al., 1988; Ran et al., 1997; Yu et al., 2019). The earthquake produced at least 10-12 km long coseismic surface rupture along the northern part of the fault (Fig. 1b), leaving fault scarps of 0.5–3.1 m high (Xiang et al., 1988; Yu et al., 2019). The Xiadian fault is an active, right-lateral strike-slip fault, possibly with some normal components. It strikes NE 39–52° and dips SE, extending over 102 km in length. Most of the fault is hidden by thick loose Quaternary sediments, except the northern part (Fig.1b). The Xiadian fault appears to play a principal role in controlling the formation and progression of the (half)graben located to the east, specifically the Langfang-Dachang depression. Seismic data reveal that the graben has accumulated over 3 kilometers of Cenozoic sedimentary layers, along with more than 600 meters of Quaternary deposits (Xiang et al., 1988). Paleoseismic studies reveal that large earthquakes (M≥7) on the Xiadian fault have a recurrence interval between ~2,800 yr (Yu et al., 2019) and ~6,500 yr (Ran et al., 1997) during the last 200 ka.

The Hexiwu fault is a ~80 km long, NNE-striking buried fault that subparallel to the Xiadian fault (Fig. 1b). The Hexiwu fault can be divided into northern and southern sections by the nearly E-W striking Baodi fault. A 4–6 km long stepover is developed between these two sections. The northern section (also called the Xianghe fault) dips NW and probably merge with the Xiadian fault at depth (Liu et al., 2009). Seismic reflection data and boreholes suggest that the southern section dips SE, which may control the formation and evolution of the (half)graben to the east, i.e., the Wuqing depression (Zhao et al., 2013). Up to 700m of Quaternary sediments were accumulated in the depression (Zhao et al., 2013).

3. Data analysis and results

The seismic waveform data used in this study comprise: (1) velocity waveforms recorded by the permanent China Earthquake Monitoring Network (black triangles in Fig. 1a), and (2) acceleration waveforms from the National Earthquake Early Warning Network (blue triangles in Fig. 1a), which was deployed in the Beijing-Tianjin-Hebei region in June 2021. Earthquake catalog was obtained from the CENC (http://10.5.160.18). During the study period (26 March to 31 May 2025), the catalog recorded 17 aftershocks of the 2025 Yongqing M_L4.6 earthquake, including 1 event $M_L \geq 3.0$ and 3 $M_L \geq 2.0$.

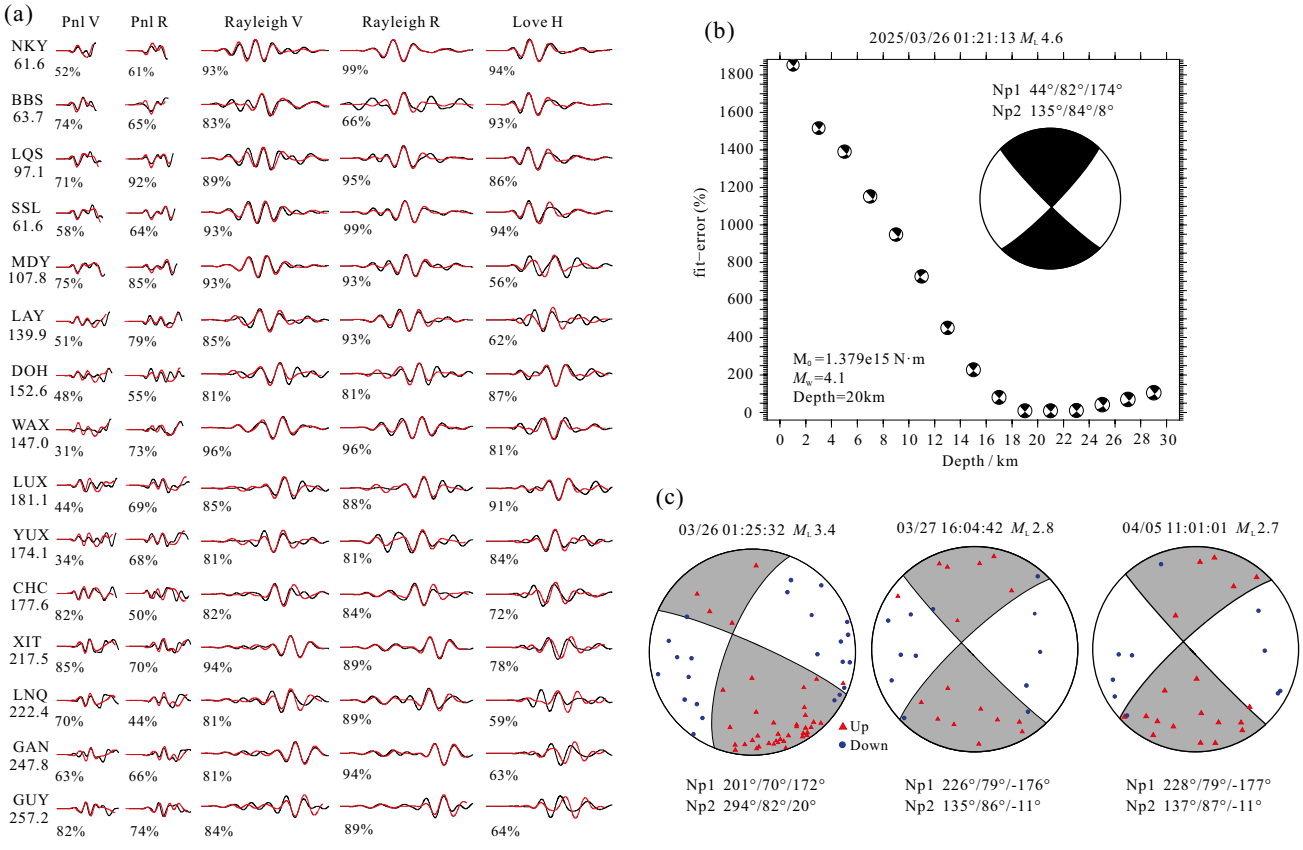

Figure 2. (a) Waveforms fitting results by CAP inversion for the 2025 Yongqing M_L4.6 mainshock. Station names are annotated with epicentral distances (km), and the cross-correlation coefficients between observed (black) and synthetic (red) waveforms are provided below each comparison. (b) The misfit variations as a function of centroid depth. (c) Focal mechanisms of the three $M_L \geq 2.5$ aftershocks based on the P-wave polarities.

Focal mechanism

We inverted the focal mechanism, seismic moment, and centroid depth of the M_L4.6 mainshock by the Cut-And-Paste (CAP) method (Zhu and Helmberger, 1996). Broadband seismic waveforms from stations in Fig. 1a were separated into P and surface wave segments, which independently time-shifted to minimize the uncertainties due to velocity models. The waveforms were band-pass filtered at 0.05-0.2 Hz (P) and 0.05-0.1 Hz (surface waves). Green's functions were computed via the frequency-wavenumber (f-*k*) method (Zhu and Rivera, 2002) by the Crust2.0 velocity model. The results are presented in Fig. 2a and Fig. 2b. The moment magnitude is M_W4.1, seismic moment (M_0) is 1.379×10^{15} Nm, with nodal planes (strike/dip/rake) of 44º/82º/174º (NP1) and 135º/84º/8º (NP2), and a focal depth of 20 km.

Focal mechanisms for the three $M_L\geq2.5$ aftershocks were independently determined by the CHNYTX program (Yu et al., 2010) based on the P-wave polarities, which incorporates manual picking of polarities from clear initial motions, and waveform correlation derived polarities (Shelly et al., 2016) for accelerometer records with ambiguous first motions. The results (Fig. 2c) reveal consistent strike-slip mechanisms for all events, which is left-lateral strike-slip with NE strike (NP1) and right-lateral strike-slip with NW strike (NP2).

Earthquake detection and relocation

This paper adopted the matched-filter technique (Peng and Zhao, 2009) to detect potential missing events in the catalog. The analysis utilized high signal-to-noise ratio waveforms from three accelerometers and one seismometer, which selected the mainshock and nine cataloged earthquakes ($M_L\geq1.5$) as templates. Continuous data and templates were band-pass filtered at 2-10 Hz to enhance high-frequency signals. Template waveforms (3-component) were extracted from 1 s before to 3 s after the S-wave arrival. Cross-correlation scanning of continuous data (26 March to 31 May 2025) identified detections when the average cross-correlation coefficient (CC) across stations exceeded 9 times of the median absolute deviation (MAD), or the CC at any single station surpassed 0.7 for at least two templates. This paper detected 4 events missing from the catalog, including only 1 event with magnitude $M_L\geq1.0$ (M_L1.1) occurred about 2 minutes after the mainshock.

Earthquakes were relocated using double-difference method (HypoDD, Waldhauser and Ellsworth, 2000) with the velocity model in Table 1. Initially, the relative locations of the 2018 and 2025 mainshocks were determined by seismic records from seismometers situated within an epicentral distance of 100 km. Subsequently, the 2025 mainshock and aftershocks with ML≥1.0 were relocated employing data from accelerometers located within 50 km and seismometers within 100 km of the epicenter. Initial locations for 2025 sequence were constrained with the mainshock epicenter from the CENC catalog and a fixed centroid depth of 20 km determined by CAP inversion (Fig. 2b). Given the high waveform similarity between the mainshock and aftershocks revealed by template matching, we chose the M_L3.4 aftershock as template (detected the largest number of earthquakes in template matching) with all phase picks were manually verified, and calibrated the arrival times of the 2025 mainshock and other aftershocks by waveform cross-correlation. The singular value decomposition (SVD) method was selected to solve the DD equations, which adequately represents least squares errors in relocation result (Waldhauser and Ellsworth, 2000).

Table 1. Seismic wave velocity model in study area

Depth of upper interface (km)	P-wave velocity (km s^{-1})	S-wave velocity (km s^{-1})
0	3.0	1.5
3	5.9	3.4
10	6.1	3.5
15	6.2	3.6
20	6.4	3.7
30	6.6	3.8
34	8.0	4.6

The relocated hypocenters are shown in Figure 3. The 2018 mainshock is in the southeast direction of the 2025 mainshock (Fig. 3a), with the epicentral distance of about 11km, and the focal depth of the 2018 mainshock is shallower (Fig. 3b). In map view of 2025 earthquake sequence (Fig. 3c), the epicenters exhibit a predominant NE-SW alignment. To assess their spatial relationship with the mainshock's focal mechanism, this paper projected the hypocenters onto two cross-sections oriented along the strikes of the nodal planes: profile BB' (45°) and profile CC' (135°). The CC' profile (Fig. 4e) reveals a well-defined near vertical linear distribution, which correlates well with the geometry of NP1 (strike=44°, dip=82°) in the focal mechanism solution (Fig. 2b). This alignment suggests that NP1 represents the likely rupture plane.

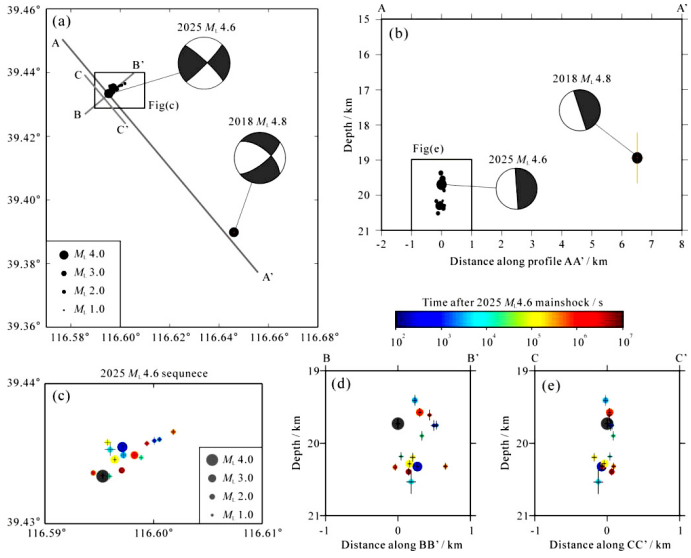

Figure 3. (a) Map view of the relocated earthquakes of 2025 M_L4.6 earthquake sequence and 2018 M_L4.8 mainshock. The magnitude scale is shown in the legend. The strikes of profiles AA' (45°), BB' (135°) and CC' (45°) refer to the focal mechanism nodal planes. (b) Epicenter projection distribution along profile AA'. The orange cross represents the location error of 2018 M_L4.8 mainshock. The focal mechanism of 2018 M_L4.8 mainshock is from Zhang et al (2018). (c) Map view of the relocated 2025 earthquake sequence. The magnitude scale is shown on the right. (d) Epicenter projection distribution along profile BB'. (e) Same as (d) but for profile CC'. The black crosses represent the relocation errors of 2025 earthquake sequence from HypoDD by SVD method.

Rupture direction

To better constrain the seismogenic structure, we analyzed the rupture direction of the mainshock using two independent methods.

(1) Centroid relative relocation

During waveform cross-correlation processing, consistent temporal discrepancies were identified between calibrated P-wave arrival times obtained through waveform cross-correlation and those determined via manual picking across multiple stations. These time delays reflect the spatial separation between the hypocenter and the centroid (Xu and Wen, 2019), which determines the rupture direction (hypocenter to centroid). Figure 4 illustrates the time delay calculation methodology by station XOX as an example. Firstly, the vertical component waveforms of the M_L4.6 mainshock and M_L3.4 aftershock are band-pass filtered at 0.05-40Hz. A 11-sample window of ±5 samples around the M_L3.4 aftershock's P-wave arrival time was extracted with pre-P-wave noise was suppressed by 10 times amplitude attenuation. The P-wave arrival time of the mainshock is aligned by comparing with the 11-sample length waveform of the mainshock and M_L3.4 aftershock (Fig. 4b). Then, the vertical component waveforms were reprocessed with a 2-10 Hz band-pass filter, and 1.0 s segments (0.3 s pre- to 0.7 s post-P arrival) were intercepted. The cross-correlation function was computed at 100× interpolated resolution. The time delay between the peak and zero measurements was preserved exclusively in cases where the function exhibited a single prominent peak and the peak value ≥0.7 (Fig. 4c).

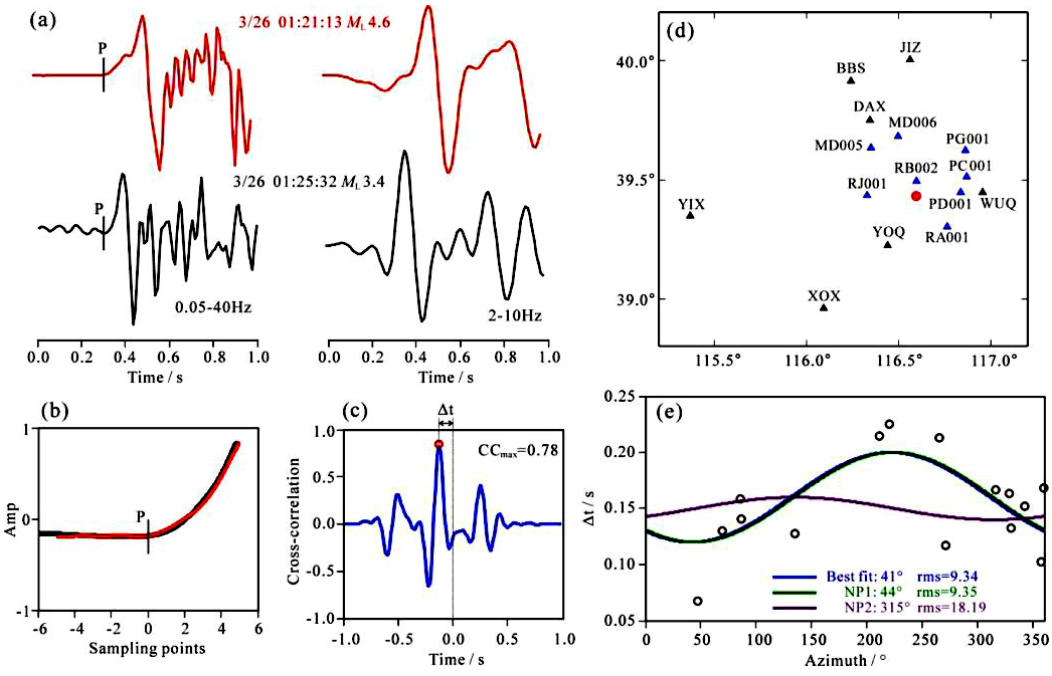

Figure 4. The calculation methodology of P-wave arrival time delay and rupture direction analysis result. (a) The vertical component P-wave waveforms of the M_L4.6 mainshock (red) and M_L3.4 aftershock (black) band-pass filtered at 0.05-40Hz and 2-10Hz. (b) Comparison of the 11-sample length waveforms filtered at 0.05-40Hz of the mainshock (red) and M_L3.4 aftershock (black). (c) The waveform cross-correlation (CC) function of mainshock and M_L3.4 aftershock filtered at 2-10Hz. The time delay is measured from the difference between peak (red circle) and zero. (d) Distribution of the stations with CC ≥ 0.7. Red circle is the epicenter of M_L4.6 mainshock, and triangles represent accelerometers (blue) and seismometers (black) with station name above. (e) Fitting results of the time delays with azimuth for rupture direction analysis. The blue line represents the best-fit curve by Equation (1), while the purple and green lines denote the fit curves assuming the rupture direction angles as the strikes of NP1 and NP2 from the focal mechanism, respectively. Fitting errors are provided in the lower part of the figure.

This paper got the time delay results of 15 stations (Fig. 4d), including 7 seismometer stations and 8 accelerometer stations. The time delay δt at each station can be written as follows.

$$\delta t = t_0 - \frac{\Delta \bullet \cos(\theta)}{c} \quad (1)$$

where t_0 represents the time difference associated with rupture velocity, rupture length, and the rise time of the source time function. Δ denotes the rupture distance. θ is the azimuth of the station relative to the rupture direction, and c is the S-wave velocity near the source (Wu et al., 2019; He et al., 2021). When θ=0, δt reaches its minimum value, and the azimuth is the rupture direction. The fitting result (Fig. 4e) shows an optimal rupture azimuth of 41°with a misfit value of 9.34. For comparison, this paper evaluated the misfits for the nodal plane strikes from focal mechanism obtained from P-wave polarities. NP1 (strike 44°/224°) has a misfit of 9.35, while NP2 (strike 315°/135°) shows significantly larger misfit of 18.19. The optimal rupture direction (41°) agrees well with the strike of NP1 (44°), and the lower misfit for NP1 means that the rupture of the 2025 Yongqing earthquake likely propagates in SW-NE direction.

(2) Spectral ratio analysis

Different shapes of spectral ratio curves may relate to the direction of earthquake rupture (Wu et al. 2019). Using multi-window spectral ratio method (Huang et al., 2016), we calculated the spectral ratio of M_L4.6 mainshock and M_L3.4 aftershock. The spectral ratio curves exhibit two distinct patterns. In the directivity-type (Fig. 5b), the curve with valley and peak means in 3-5Hz and 5-10Hz respectively, and the isotropic-type (Fig. 5c) is relatively smooth in 1-10 Hz matching the Boatwright source model. The directivity-type curves are analogous to characteristics of forward-rupture stations' curves in Wu et al. (2019). Notably, the directivity-type stations cluster NE of the epicenter (Fig. 5d) indicate a SW-to-NE rupture propagation of the mainshock, which is consistent with the result based on P-wave time delays (Fig. 4e).

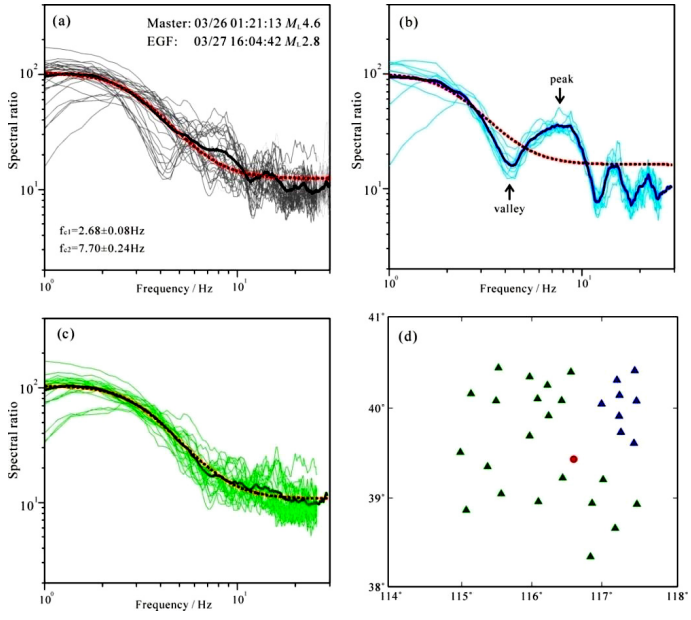

Figure 5. Rupture direction analysis of the mainshock using spectral ratio analysis. Spectral ratios adopt individual EGF events (thin solid lines) and their logarithmic stack (thick solid line) for all stations (a), the directivity-type (b) and the isotropic-type (c), respectively. The red dashed curve shows the best fitting by Boatwright model. (d) Distribution of stations with spectral ratio in the directivity-type (blue) and the isotropic-type (green).

4. Discussion

Integrated seismological analysis constrains the geometry and kinematics of the seismogenic fault of the 2025 Yongqing earthquake sequence. Relocation of earthquakes reveals a near-vertical fault plane that strikes NE (Fig. 3), which agrees well with the NP1 from our focal mechanism solution of the M_L4.6 mainshock (Fig. 2). A NE-striking seismogenic fault is further confirmed by two independent rupture direction analysis, which both consistently represent SW-to-NE rupture propagation (Figs. 4 and 5). Focal mechanism inversion demonstrates predominant right-lateral strike-slip motion along this NE-striking plane, with a minor normal component (Fig. 2). Collectively, the seismological analysis results indicate that the seismological structure of the 2025 Yongqing M_L4.6 earthquake is likely a high-angle, SE-dipping right-lateral strike-slip fault, and the rupture propagation direction may be SW-NE direction.

Comparing with Zhang et al (2018) and Li et al (2020), the 2025 Yongqing M_L4.6 earthquake shares kinematic similarities with the 2018 M_L4.8 earthquake, including comparable focal depths (19-20 km) and rupture mechanisms—both occurred on high-angle, NE-striking, right-lateral strike-slip faults, despite an ~11 km epicentral separation. Two (N)NE-striking faults—the Hexiwu and Xiadian faults—are located near the epicenters of the 2018 and 2025 Yongqing earthquakes. The southern segment of the Hexiwu fault, located to the west of both seismic events, displays a southeastward dip, which is incongruent with the previously inferred high-angle geometry of the seismogenic fault associated with the Yongqing earthquakes (Fig. 6). In contrast, the Xiadian fault is a complex zone comprising both shallowly SE-dipping faults and steeply dipping structures extending to the Moho (Liu et al., 2009). The steeply dipping fault geometries inferred from seismic analysis of the Yongqing earthquakes correspond closely with the deeper structural characteristics of the Xiadian fault zone. Nevertheless, considering the hypocentral separation exceeding 10 km between the Yongqing earthquake sequence and the Xiadian Fault (Fig. 1b), a definitive correlation between these seismic events and the steeply dipping fault observed in reflection profiles cannot be established. Instead, we propose that the seismogenic structures of the Yongqing earthquakes are secondary faults of the Xiadian fault, which are antithetical and merged with the latter at depth (Fig. 6). The two moderate and other smaller earthquakes in the Yongqing area may reflect the stress adjustment of the Xiadian fault system.

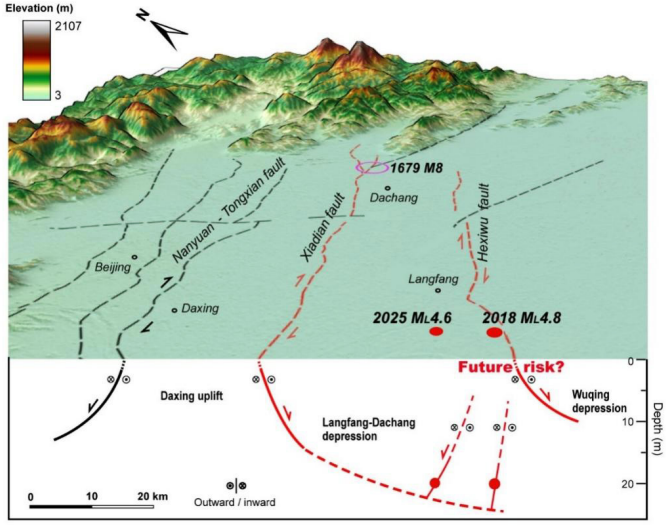

Figure 6. Block diagram showing the seismogenic structures of the two Yongqing earthquakes and the relationship with the Xiadian fault (the causative fault of the 1679 Sanhe-Pinggu M8 earthquake). The seismogenic structures of the two earthquakes are possibly secondary faults that are antithetical and merged with the Xiadian fault at depth. The Hexiwu fault may be a potential seismic risk in the future. The geometry of the Xiadian fault is modified from Fig.4 of Zhao et al. (2013), but note that we have adjusted the coordinate scale to 1:1, thus the fault looks flatter in the deep than the original version.

Historical and instrumental seismicity in the North China Plain reveals that most of the strong earthquakes ($M \geq 6.5$) have occurred on NE- to NNE-striking faults over the past two millennia, with only a few exceptions on NW- to NNW-striking structures (e.g., the 1830 Cixian M ~7.5 and 1975 Haicheng M 7.3 earthquakes) (Liu et al., 2007; 2011). This spatial distribution aligns with the active tectonic regime of the North China Plain, which dominated by NE-NNE-striking right-lateral strike-slip faults, with subordinate NW-NNW-striking left-lateral faults (Chen et al., 1988; Lei et al., 2022). The Xiadian and Hexiwu faults exemplify this NE-NNE right-lateral system. The two Yongqing moderate earthquakes have similar kinematic mechanism with two major historical earthquakes in the North China Plain, the 1966 Xingtai M 7.2 and 1976 Tangshan M 7.8 earthquakes, which also ruptured (N)NE-striking right-lateral strike-slip faults (Huang & Yeh, 1997; Chen et al., 1975). A similar mechanism is observed for the 2006 Wen'an M_S5.1 earthquake (Huang et al., 2009), ~14 km SW of the 2025 Yongqing event, where the NE-striking nodal plane exhibits right-lateral slip, though the causative fault remains debated. Collectively, the focal mechanisms of these moderates to large earthquakes correspond with the current crustal stress pattern in the North China Plain, characterized by NE-SW compression and NW-SE extension, as indicated by geodetic data (Shen et al., 2000) and/or focal mechanisms of smaller earthquakes (Lin et al., 2007).

The Xiadian fault was the seismogenic structure of the 1679 Sanhe-Pinggu M~8 earthquake (Xiang et al., 1988; Ran et al., 1997; Yu et al., 2019). Paleoseismic study reveals that large earthquakes (M≥7) on the Xiadian fault have a long recurrence interval (2,800-6,500yr) (Ran et al., 1997; Yu et al., 2019). Therefore, it seems that the seismic risk along the Xiadian fault is not imminent. However, the Hexiwu fault appears to need more caution. Recent shallow seismic survey and drilling data show that the Hexiwu fault is a Late Pleistocene active fault (Yan Chengguo, 2025, Tianjin Earthquake Agency, personal communication). More than 700m of Quaternary sediments has accumulated in the Wuqing depression bounded by the Hexiwu fault (Zhao et al., 2013). The only earthquake known to have occurred on the Hexiwu Fault in the last thousand years is a M ~5.5 event in A.D. 1621 according to the Chinese Historical Earthquake Catalogue (Li and Li, 2021). Using the empirical relationship between fault length L (~80 km) and moment magnitude (M_W) for strike-slip faults (Wells and Coppersmith, 1994): $M_w = (5.16 \pm 0.13) + (1.12 \pm 0.08) * \lg L$, the Hexiwu fault could host earthquakes with a maximum magnitude of M_W6.5-7.0.

5. Conclusions

Seismological analysis reveals that the 2025 Yongqing M_L4.6 earthquake ruptured a NE-striking, nearly vertical right-lateral strike-slip fault, which is very similar to the 2018 Yongqing M_L4.8 event. The seismogenic structure of the 2025 and 2018 Yongqing earthquakes are secondary faults of the Xiadian fault, which are antithetical and merged with the latter at depth. Along with other smaller earthquakes in the Yongqing area, these two moderate magnitude earthquakes, may reflect the stress adjustment of the Xiadian fault system. The Hexiwu fault is likely a potential seismic risk in North China Plain that could be capable of generating a M_W6.5-7.0 earthquake in the future.

References

Chen, W. P., & Nábelek, J. (1988). Seismogenic strike-slip faulting and the development of the North China Basin. *Tectonics*, 7(5), 975–989. https://doi.org/10.1029/TC007i005p00975

Chen, Y. T., Lin, B. H., Lin, Z. Y., & Li, Z. Y. (1975). The focal mechanism of the 1966 HSINGTAI earthquake as inferred from the ground deformation observations. *Chinese Journal of Geophysics*, 18(3), 164–182. https://doi.org/10.1002/cjg2.v18.3

Feng, J. K., Yao, H. J., Chen, L., & Li, C. L. (2022). Ongoing lithospheric alteration of the North China Craton revealed by surface-wave tomography and geodetic observations. *Geophysical Research Letters,* 49, e2022GL099403. https://doi.org/10.1029/2022GL099403

He, X. H., Liang, H., Zhang, P. Z., & Wang, Y. (2025). The 2019 MS4.2 and 5.2 Beiliu earthquake sequence in South China: Complex conjugate strike-slip faulting revealed by rupture directivity analysis. *Seismological Research Letters,* 92(6), 3327–3338. https://doi.org/10.1785/0220210176

Huang, B. S., & Yeh, Y. T. (1997). The fault ruptures of the 1976 Tangshan earthquake sequence inferred from coseismic crustal deformation. *Bulletin of the Seismological Society of America,* 87(4), 1046–1057. https://doi.org/10.1785/BSSA0870041046

Huang, J. P., Ni, S. D., Fu, R. S., Niu, F. L., Shao, Z. G., & Zheng, Y. (2009). Source mechanism of the 2006 Mw5.1 Wen'an Earthquake determined from a joint inversion of local and teleseismic broadband waveform data. *Chinese Journal of Geophysics,* 52(1), 120–130. https://doi.org/10.1002/cjg2.1327

Huang, W. Q., Li, W. X., & Cao, X. F. (1994). Research on the completeness of earthquake data in the Chinese mainland (I) — North China. *Acta Seismologica Sinica*, 7(3), 351–359. https://doi.org/10.1007/BF02666301

Huang, Y. H., Beroza, G. C., & Ellsworth, W. L. (2016). Stress drop estimates of potentially induced earthquakes in the Guy-Greenbrier sequence. *Journal of Geophysical Research: Solid Earth,* 121, 6597–6607. https://doi.org/10.1002/2016JB013067

Lei, S. X., Liu, J. B., Weldon, R. J., Liu, S. Q., Qiu, H., Song, T., Wang, X. S., Zhao, S. D., & Yan, C. G. (2022). Seismogenic structure of the 1976 Ninghe (Tianjin) MS6.9 earthquake and its tectonic implications. *Quaternary Sciences,* 42(3), 755–767. https://doi.org/10.11928/j.issn.1000-0550.2022.03.011

Li, H., Dong, Y. B., Wang, Y. X., Peng, Y. F., Liu, S. Q., & Wu, B. Y. (2020). Seismological evidence for a deep-seated shear zone in the Langgu Depression. *Chinese Journal of Geophysics,* 63(2), 492–504. https://doi.org/10.6038/cjg2020N0192

Li, L., Chen, Q. F., Cheng, X., & Niu, F. L. (2007). Spatial clustering and repeating of seismic events observed along the 1976 Tangshan fault, North China. *Geophysical Research Letters,* 34(23), L23309. https://doi.org/10.1029/2007GL031594

Li, W., & Li, J. (2021). *Study on historical earthquakes in China.* Seismological Press.

Lin, X. D., Yuan, H. Y., Xu, P., Yang, X., Xu, Z. G., Sun, H. X., Hou, L. J., Xu, S. T., & Xi, C. X. (2017). Zonational characteristics of earthquake focal mechanism solutions in North China. *Chinese Journal of Geophysics,* 60(12), 4589–4622. https://doi.org/10.6038/cjg20171206

Liu, B. J., Hu, P., Meng, Y. Q., Feng, S. Y., Shi, J. H., & Ji, J. F. (2009). Research on fine crustal structure using deep seismic reflection profile in Beijing region. *Chinese Journal of Geophysics*, 52(9), 2264–2272. https://doi.org/10.3969/j.issn.0001-5733.2009.09.010

Liu, M., Stein, S., & Wang, H. (2011). 2000 years of migrating earthquakes in north China: How earthquakes in mid-continent differ from those at plate boundaries. *Lithosphere,* 3(2), 128–132. https://doi.org/10.1130/L129.1

Liu, M., Yang, Y. Q., Shen, Z. K., Wang, S. M., Wang, M., & Wan, Y. G. (2007). Active tectonics and intracontinental earthquakes in China: The kinematics and geodynamics. *The Geological Society of America Special Paper,* 425, 299–318. https://doi.org/10.1130/0-8137-2425-5.299

Peng, Z. G., & Zhao, P. (2009). Migration of early aftershocks following the 2004 Parkfield earthquake. *Nature Geoscience*, 2, 877–881. https://doi.org/10.1038/ngeo697

Ran, Y. K., Deng, Q. D., Yang, X. P., Zhang, W. X., Li, R. C., & Xiang, H. F. (1997). Paleoearthquakes and recurrence interval of the seismogenic fault of 1679 Sanhe-Pinggu M8 earthquake, Hebei and Beijing. *Seismology and Geology,* 19(3), 193–201. https://doi.org/10.3969/j.issn.0253-4967.1997.03.001

Shen, Z. K., Zhao, C. K., Yin, A., Li, Y. X., Jackson, D. D., Fang, P., & Dong, D. (2000). Contemporary crustal deformation in east Asia constrained by Global Positioning System measurements. *Journal of Geophysical Research: Solid Earth,* 105(B3), 5721–5734. https://doi.org/10.1029/1999JB900391

Shelly, D. R., Hardebeck, J. L., Ellsworth, W. L., & Hill, D. P. (2026). A new strategy for earthquake focal mechanisms using waveform-correlation-derived relative polarities and cluster analysis: Application to the 2014 Long Valley Caldera earthquake swarm. *Journal of Geophysical Research: Solid Earth,* 121, 8622–8641. https://doi.org/10.1002/2016JB013437

Waldhauser, F., & Ellsworth, W. L. (2000). A double-difference earthquake location algorithm: Method and application to the northern Hayward Fault, California. *Bulletin of the Seismological Society of America,* 90(6), 1353–1368. https://doi.org/10.1785/0120000006

Wells, D. L., & Coppersmith, K. J. (1994). New empirical relationships among magnitude, rupture length, rupture width, rupture area, and surface displacement. *Bulletin of the Seismological Society of America,* 84(4), 974–1002. https://doi.org/10.1785/BSSA0840040974

Wu, Q. M., Chen, X. W., & Abercrombie, R. E. (2019). Source complexity of the 2015 Mw4.0 Guthrie, Oklahoma earthquake. *Geophysical Research Letters,* 46(9), 4674–4684. https://doi.org/10.1029/2019GL082238

Xiang, H. F., Fang, Z. J., Xu, J., Li, R. C., Jia, S. F., Hao, S. J., Wang, J. B., & Zhang, W. X. (1988). Study on tectonic setting and earthquake repeatability in Sanhe-Pinggu earthquake zone. *Seismology and Geology,* 10(1), 15–28. https://doi.org/10.3969/j.issn.0253-4967.1988.01.002

Xu, Y. Y., & Wen, L. X. (2019). Relative directivity inversion of small earthquake rupture. *Geophysical Journal International,* 218, 631–639. https://doi.org/10.1093/gji/ggz183

Yin, A., Yu, X. J., Shen, Z. K., & Liu-Zeng, J. (2015). A possible seismic gap and high earthquake hazard in the North China Basin. *Geology,* 43(1), 19–22. https://doi.org/10.1130/G36155.1

Yu, C. Q., Tao, K., Cui, X. F., Hu, X. P., & Ning, J. Y. (2009). P-wave first-motion focal mechanism solutions and their quality evaluation. *Chinese Journal of Geophysics,* 52(5), 1402–1411. https://doi.org/10.1002/cjg2.52.5.1402

Yu, Z. Y., Pan, H., Xi, H., Zhang, Y. H., & Chen, H. (2019). Late Quaternary paleoseismicity of the Xiadian fault in the North China Plain with implications for earthquake potential. *Journal of Asian Earth Sciences,* 184, 103997. https://doi.org/10.1016/j.jseaes.2019.103997

Zhang, P. Z., Deng, Q. D., Zhang, G. M., Ma, J., Gan, W. J., Min, W., Mao, F. Y., & Wang, Q. (2003). Active tectonic blocks and strong earthquakes in the continent of China. *Science China Series D: Earth Sciences,* 46, 13–24. https://doi.org/10.1360/03yd0002

Zhang, Y., Chen, Y. T., & Song, J. (2018). Source mechanism and rupture characteristics of the 2018 Mw4.3 Yongqing earthquake. *Chinese Science Bulletin*, 63(22), 2296–2301. https://doi.org/10.1360/N972018-00229-6

Zhao, C. B., Liu, B. J., Ji, J. F., Feng, S. Y., & Shi, J. H. (2023). Fine crustal structure in the south of Beijing revealed by deep seismic reflection profiling. *Chinese Journal of Geophysics*, 56(4), 1168–1176. https://doi.org/10.6038/cjg20130406

Zhu, L. P., & Helmberger, D. V. (1996). Intermediate depth earthquakes beneath the India-Tibet Collision Zone. *Geophysical Research Letters*, 23(5), 435–438. https://doi.org/10.1029/96GL00165

Zhu, L. P., & Rivera, L. A. (2002). A note on the dynamic and static displacements from a point source in multilayered media. *Geophysical Journal International,* 148, 619–627. https://doi.org/10.1046/j.1365-246X.2002.01632.x